Quinazolinone derivatives as selective COX-2 inhibitors: *In silico* analysis using molecular docking, dynamics, and ADMET

Tendy Oktriawan, Tri Joko Raharjo ⬤, Winarto Haryadi, Muhammad Idham Darussalam Mardjan*⬤

Department of Chemistry, Faculty of Mathematics and Natural Sciences, Universitas Gadjah Mada, Yogyakarta, Indonesia.

ABSTRACT

The cyclooxygenase-2 (COX-2) is an enzyme frequently overexpressed in cancer cells, making it a promising target for the preliminary screening of anticancer agents. The development of effective COX-2 inhibitors is crucial for advancing cancer therapy. This study aimed to evaluate the potential of quinazolinone derivatives as COX-2 inhibitors using *in silico* approaches, focusing on their structural modifications and pharmacokinetic properties. We designed and optimized 30 quinazolinone derivatives with various aromatic substituents using the DFT-B3LYP-6-31G(d,p) level of theory. Molecular docking and molecular dynamics simulations were performed to assess their binding affinity and stability within the COX-2 active site. In addition, absorption, distribution, metabolism, excretion, and toxicity (ADMET) predictions were conducted to evaluate their pharmacokinetic properties. The molecular docking results showed that benzylated quinazolinones exhibited stronger binding energies compared to phenylated ones. Specifically, methoxy (compound **5**) and trifluoromethyl (compound **8**) substituents at the *para*-position formed hydrogen bonds with key residues in the COX-2 active site. Molecular dynamics simulations confirmed the stability of these compounds during a 100 ns simulation. The molecular mechanics Poisson–Boltzmann surface area analysis indicated a higher binding energy for methoxy-substituted quinazolinones (compound **5**). ADMET predictions revealed favorable pharmacokinetic properties for benzylated quinazolinones with methoxy and trifluoromethyl groups. This study highlights the potential of benzylated quinazolinones with methoxy and trifluoromethyl groups as a promising anticancer agent against COX-2.

1. INTRODUCTION

Cancer remains one of the most devastating diseases globally, with a rapidly growing burden [1]. The World Health Organization predicts that by 2050, there will be over 35 million new cancer cases, marking a 77% increase from the estimated 20 million cases in 2022 [2–4]. Despite significant advancements in chemotherapy, the development of new anticancer agents often faces challenges due to the complexity of cancer biology and the emergence of drug resistance [5,6]. Therefore, this alarming rise underscores the urgent need for innovative and effective cancer therapies.

Rational drug design, leveraging computational chemistry approaches, has emerged as a promising strategy for rapidly screening and identifying potential anticancer compounds [7]. This method involves selecting specific protein targets, performing molecular docking, conducting molecular dynamics simulations, and evaluating absorption, distribution, metabolism, excretion, and toxicity (ADMET) profiles to identify the most promising candidates [8].

The cyclooxygenase-2 (COX-2) is a critical enzyme frequently overexpressed in various types of tumors, playing a pivotal role in cancer progression and resistance to conventional therapies. Its multifaceted role in cancer involves promoting tumor growth, immune evasion, and resistance to therapies [9]. COX-2 achieves these effects by producing Prostaglandin E2, which activates key signaling pathways such as the Mitogen-Activated Protein Kinase and Phosphoinositide 3-Kinase / Protein Kinase B pathways, leading to enhanced cell proliferation, angiogenesis,

*Corresponding Author

Muhammad Idham Darussalam Mardjan, Department of Chemistry,
Faculty of Mathematics and Natural Sciences, Universitas Gadjah Mada,
Yogyakarta, Indonesia. E-mail: idham.darussalam @ ugm.ac.id

and metastasis [10]. In addition, COX-2 promotes cancer stem cell-like behavior, enhances cell survival, and facilitates inflammation [11]. The strategic use of COX-2 inhibitors has been shown to enhance the efficacy of other cancer treatments, such as radiotherapy and chemotherapy, by sensitizing cancer cells to these therapies [12]. Moreover, computational docking analyses have revealed that several compounds exhibit strong binding affinities to the COX-2 active site, suggesting effective inhibition of the enzyme. This inhibition is significant because the overexpression of COX-2 is often associated with cancer progression [13,14]. Therefore, targeting COX-2 has become a crucial approach in the development of novel anticancer agents, offering potential synergies with existing therapies to improve treatment outcomes [15].

Heterocyclic compounds, particularly quinazolinones, have garnered significant attention due to their diverse pharmacological activities, such as anticancer [16], anticonvulsant [17], antimalarial [18], antifungal [19], antibacterial [20], anti-inflammatory [21], MMP inhibitors [22], antidiabetic, and antileishmanial agents [23]. Quinazolinones have been explored extensively for their therapeutic potential, with several derivatives exhibiting promising anticancer activities against various cancer cell lines [24,25]. Notably, some quinazolinone derivatives have shown potent inhibition of the COX-2 enzyme, highlighting their potential as selective anticancer agents [26].

Most existing *in silico* studies on quinazolinone derivatives as anticancer agents focus on broad mechanisms and often target enzymes like EGFR or tyrosine kinases. However, these approaches frequently lead to significant side effects and suboptimal pharmacokinetic profiles [27,28]. In contrast, this research specifically examines the molecular binding affinity of quinazolinone derivatives to COX-2, aiming to identify compounds with strong selectivity, optimal pharmacokinetics, and minimal side effects. This study aims to address this gap by evaluating a series of quinazolinone compounds with diverse functional groups, such as –OH, -OCH$_3$, -Cl, -CH$_3$, -NO$_2$, -Br, and -thiophene, as COX-2 inhibitors. Previous reports have shown the promising activities of quinazolinone derivatives, including anticancer effects against the MCF-7 cell line with logIC$_{50}$ values ranging from 0.66 to 3.93 μM [29,30], and inhibition of the COX-2 enzyme with IC$_{50}$ values of 0.04 to 63 μM with a selectivity index of 373.77 [31,32]. This study screened 30 quinazolinone derivatives via molecular docking to identify potential COX-2 inhibitors, with the top-performing compounds further analyzed through molecular dynamics simulations to evaluate binding stability, complemented by ADMET predictions to assess drug-likeness and safety profiles. Through molecular docking, molecular dynamics simulations, and ADMET predictions, this research explores the structural modifications and pharmacokinetic properties of these compounds to contribute to the development of novel, effective, and safer anticancer therapies targeting COX-2.

2. MATERIALS AND METHODS

2.1. Materials

The three-dimensional (3D) single-crystal structure of COX-2 (PDB ID: 3LN1) was obtained from the Research Collaboratory for Structural Bioinformatics Protein Data Bank website https://www.rcsb.org. Celecoxib was used as the native ligand. Thirty quinazolinones served as the ligand models for the study. Computational analyses were conducted using a computer equipped with an Intel® Xeon processor CPU E5-2650 v2@2.60 GHz. The software used in this study includes GaussView version 5.0, Gaussian 09 Revision D.01, Chimera version 1.13.1, AutoDockTools version 1.5.6 [33], AutoDock version 4.2.6, Discovery Studio Visualizer 2019 [34], and Yasara-Structure version 23.8.19 [35], with computational resources supported by the Austrian-Indonesian Center for Computational Chemistry at Universitas Gadjah Mada.

2.1. Procedure

2.1. Molecular docking of quinazolinone derivatives

The molecular docking protocol in this study was conducted according to the procedure previously reported, with some minor modifications [36]. The COX-2 receptor from *M. musculus* was prepared using Chimera. Initially, non-standard residues such as water molecules and native ligands were removed from the PDB ID: 3LN1 file [37]. Hydrogen atoms were then added to the protein to make it suitable for docking. The 3D structures of quinazolinone derivatives (1–30) were drawn using GaussView 5.0 and optimized using the DFT-B3LYP-6-31G(d,p) level of theory in Gaussian 09 Revision D.01. The optimized data were saved in PDB format. Redocking was carried out using AutoDock4, with a grid box size of 40 × 40 × 40 Å, centered at coordinates (30.096, −22.559, and −15.758), and using 100 runs of the Lamarckian Genetic Algorithm (LGA). The method was deemed acceptable for further docking analysis if the root mean square deviation (RMSD) value was less than 2 Å. The 2D structures of the quinazolinone derivatives are shown in Table 1. The same parameters as the redocking analysis (grid map size and LGA) were used. All compounds were docked into the receptor binding sites.

2.2. Molecular dynamics simulation

The molecular dynamics simulation was performed using YASARA with the md_runmembrane.mcr script to guide the preparation, minimization, equilibration, and production phases. The simulation conditions were set to mimic physiological conditions: 0.9% NaCl, pH 7.4, temperature 310 K, and pressure 1 bar [38,39]. The system employed periodic boundary conditions and the AMBER14 force field [40]. Initially, the system underwent minimization using the steepest descent method, followed by simulated annealing minimization to achieve a density of 0.999 g/ml. An initial equilibration phase of 250 ps was conducted to stabilize the system. The main simulation ran for 100 ns with a time step of 2.5 fs, and snapshots were recorded every 100 ps. Post-simulation analysis utilized the md_analyze.mcr macro [41] in Yasara to determine RMSD, root mean square fluctuation (RMSF), radius of gyration (RoG), solvent accessible surface area (SASA), and dictionary of secondary structure of proteins (DSSPs) values [42,43]. In addition, the Binding Energy calculation.mcr macro command was used to evaluate the Molecular Mechanics Poisson–Boltzmann Surface Area (MMPBSA) binding energy.

2.3. Secondary structure analysis

The 3D protein model was validated through a secondary structure analysis utilizing the Ramachandran

Table 1. Molecular dynamics simulation results for celecoxib, **5**, and **8**.

Compound	RMSD (Å)	RMSF (Å)	RoG (Å)	SASA (nm²)	DSSP
Celecoxib	2.591 ± 0.147	1.149 ± 0.511	24.461 ± 0.069	23089 ± 285	Allowed region
5	2.726 ± 0.209	1.200 ± 0.489	24.545 ± 0.098	23939 ± 311	Allowed region
8	2.934 ± 0.346	1.371 ± 0.525	24.578 ± 0.083	23818 ± 325	Allowed region

(RAM) plot, which assesses the dihedral angles ψ (psi) and φ (phi) of amino acid residues. The RAM plot for the protein under study was acquired from the Protein Data Bank Summary online platform [44].

2.4. ADMET study

Drug-likeness was predicted using Lipinski's rule (The Rule of Five), Ghose, Veber, and Egan's approaches [45–47]. Molecular properties such as MW (Molecular Weight), the number of heavy atoms, HBA (Hydrogen Bond Acceptors), HBD (Hydrogen Bond Donors), rotatable bonds, molar refractivity, TPSA (Topological Polar Surface Area), and log P were predicted using SwissADME (www.swissadme.ch). A comprehensive ADMET estimation was performed using pkCSM software.

3. RESULTS AND DISCUSSION

3.1. Molecular docking of quinazolinones against COX-2 enzyme

Our study started by optimizing the chemical structures of quinazolinones using the DFT-B3LYP-6-31G(d,p) level of theory, since this method has commonly been used for quinazolinones [48]. Compound 1 was employed as the reference compound to assess the effect of various substituents on the inhibitory ability of quinazolinones against the COX-2 enzyme. The docking parameters of the quinazolinone derivatives were validated through the redocking of celecoxib as the native ligand. The RMSD value of the redocking process was found to be 0.81 Å, demonstrating that the docking parameters are acceptable [49]. Figure 1(a) shows the superimposed conformations of celecoxib before and after the redocking process, where the conformation of celecoxib was not significantly different. The chemical interactions formed between celecoxib and the active site of COX-2 are visualized in Figure 1(b). Analysis was performed on the active site using a grid box size of 40 × 40 × 40 Å, centered at coordinates (30.096, −22.559, and −15.758). The redocking process revealed that celecoxib interacted with His75 (3.00 Å), Gln178 (1.86 Å), Leu338 (2.52 Å), Ser339 (2.22 Å), Arg499 (2.25 Å), Ile503 (2.94 Å), and Phe504 (2.64 Å) through hydrogen bonding and Ser339 through a carbon–hydrogen bond. Other hydrophobic interactions with the amino acids of Val335, Tyr341, Leu345, Leu370, Trp373, Met508, Val509, and Ala513 through pi-sigma, pi-pi stacking, and pi-alkyl interactions were also found. These chemical interactions yielded a binding energy value of −6.99 kcal/mol and a binding constant of 7.49×10^{-6} μM.

The molecular docking results of quinazolinones are listed in the supplementary data. The unsubstituted quinazolinone (compound **1**) yielded a binding energy of −5.56 kcal/mol with a hydrogen bond to the Tyr341 amino acid

residue. Unfortunately, this amino acid residue was not crucial for COX-2 inhibition, as it was not found in the native ligand. To increase the inhibitory activity of quinazolinone, we introduced several functional groups, such as methoxy and halogen groups, as these moieties are crucial for the anticancer activity through the COX-2 inhibitory mechanism [50,51].

The introduction of the *N*-benzyl group remarkably increased the binding energy of quinazolinone **2** (−8.18 kcal/mol) compared to the unmodified compound **1** (−5.56 kcal/mol). However, compound **2** did not exhibit any hydrogen bonds in the active site of the COX-2 enzyme. Higher binding energies (−8.28 to −8.52 kcal/mol were observed when a methoxy group was installed into the *N*-benzyl group (compounds **3–5**). The results demonstrated that the quinazolinone bearing a methoxy group in the *para* position **5** displayed more hydrogen bonds (His75 and Arg499) than that in the *meta* (Ser516) and *ortho* (no hydrogen bond) positions. The hydrogen bond with His75, a key amino acid for the function of the COX-2 enzyme, was also observed for celecoxib. Furthermore, compound **5** generated carbon–hydrogen bonds with Phe504 and Val509, pi-sigma interactions with Ser339, and pi-pi T-shaped interactions with Leu338 and Trp373 residues.

To enhance the inhibitory activity, various halogen-substituted quinazolinones (**6–10**) were also examined. The molecular docking study showed that the iodo group **10** exhibited the strongest binding energy (−9.29 kcal/mol), followed by the bromo **9** (−8.98 kcal/mol), chloro **7** (−8.70 kcal/mol), and trifluoromethyl **8** (−8.53 kcal/mol), followed fluoro **6** (−8.14 kcal/mol) groups. Nevertheless, compounds **6**, **9**, and **10** did not generate any hydrogen bonds, while compound **7** interacted with the Tyr341 residue through a hydrogen bond, which was not essential, as aforementioned. The presence of the trifluoromethyl group in compound **8** generated three hydrogen bonds with the amino acids of His75, Ile503, and Phe504, which were found in the celecoxib, demonstrating that they are crucial residues for COX-2. In addition, compound **8** interacted with Gln178, Leu338, and Ser339 through halogen (fluorine) interactions, with Val509 through pi-sigma interaction, with Tyr371 and Trp373 through pi-pi T-shaped interactions, and with Ala502 through pi-alkyl interaction. The results also indicated that quinazolinones containing heterocyclic rings **11–12** (7.70 and −7.16 kcal/mol) and *N*-aryl-substituted-quinazolinones **13–19** (−7.65 to −8.49 kcal/mol) displayed weaker binding energy than *N*-benzyl-substituted-quinazolinones **2–10** (−8.14 to −9.29 kcal/mol).

It was reported that the quinazolinones bearing butyl substituent exhibited potential inhibitory activity against the COX-2 enzyme [52]. In this study, *N*-butyl-substituted-quinazolinone **20** possessed a binding energy value of −6.52 kcal/mol. A stronger binding energy (−8.85 kcal/mol) was
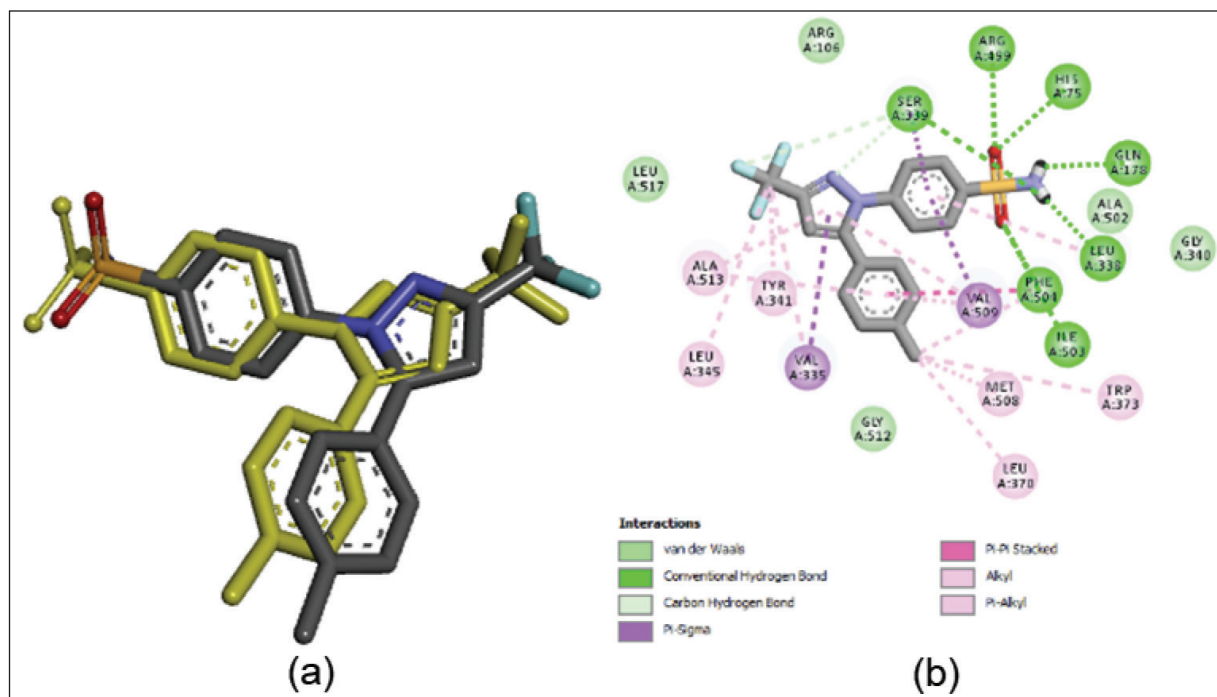
Figure 1. (a) The superimposed structure of celecoxib as the native ligand before (black) and after (gold) re-docking process. (b) The visualization of chemical interactions between celecoxib with the active site of COX-2 enzyme.

observed when *C*-aryl-substituted-quinazolinone **21** was subjected to the molecular docking study. While the presence of methyl, methoxy, and halogen groups in quinazolinone scaffolds **22–28** resulted in much stronger binding energies (ranging from −8.79 to −9.81 kcal/mol), the presence of thiophene **29** and furan **30** moieties afforded weaker binding energies (−8.42 and −7.93 kcal/mol). However, none of these compounds **20–30** generated any hydrogen bonds with crucial amino acid residues of COX-2. It was found that these compounds interacted with Tyr341 and/or Ser516, but these residues are not crucial for COX-2 inhibition activities.

Based on the molecular docking analysis, *N*-benzyl-substituted quinazolinones with para-methoxy (compound **5**) or *para*-CF$_3$ (compound **8**) groups indicated the best docking results (shown in Fig. 2), forming key hydrogen bonds and hydrophobic interactions with crucial COX-2 residues (Ile503, Phe504, His75, and Arg499), similar to those observed in the native ligand. In contrast, derivatives with other substituents did not exhibit comparable binding interactions, such as *N*-phenyl, *N*-alkyl, and *C*-phenyl.

3.2. Molecular dynamics simulations against COX-2 enzyme

The molecular docking data identified two potential quinazolinone derivatives as COX-2 inhibitors, i.e., compounds 5 and 8. Further evaluation through molecular dynamics simulation was conducted using YASARA software at 310 K for 100 ns. As illustrated in Figure 3, the RMSD value for compound **8** (2.934 ± 0.346 Å) was higher than that for compound **5** (2.726 ± 0.209 Å) and celecoxib (2.591 ± 0.147 Å). The average RMSD values did not exceed 3 Å, demonstrating that the backbone structures of quinazolinone and the COX-2 enzyme were stable during the molecular dynamics simulation. The findings reveal that compound **5** exhibits greater stability than compound **8** throughout the molecular dynamics simulation, as evidenced by its lower average RMSD value. This suggests that compound **5** maintains a more consistent binding conformation within the COX-2 active site.

In addition, the RMSF values of compound **5** (1.200 ± 0.489 Å), compound **8** (1.371 ± 0.525 Å), and celecoxib (1.149 ± 0.511 Å) were not significantly different from each other. The RMSF data indicated that residues 18, 37, 46, 58, 59, 68, 108, 155, 251, 258, 268, 344, 355, 359, 385, 391, 472, 529, 540, 563, and 569 contributed to RMSF values higher than 2 Å. From the molecular docking data, compound **5** interacted with His75 and Arg499, while compound **8** interacted with His75, Ile503, and Phe504 residues through hydrogen bondings. Fortunately, the binding poses of either compound **5** or **8** were not influenced by these unstable amino acid residues, demonstrating that the interactions of these compounds in the active site of the COX-2 enzyme remained stable.

Further Ramachandran analysis was also performed, as shown in Figure 4. The COX-2 enzyme complexed with compound **5** generated the most favored regions with 399 residues (83.6%), additional allowed regions with 70 residues (14.7%), and generously allowed regions with 6 residues (1.3%). Meanwhile, the COX-2 enzyme complexed with compound 8 generated the most favored regions with 420 residues (88.1%), additional allowed regions with 53 residues (11.1%), and generously allowed regions with 3 residues (0.6%). These results revealed that almost all regions of the COX-2 complexed with quinazolinones were located in allowed regions according to the Ramachandran plot. The DSSP of each ligand in the active site
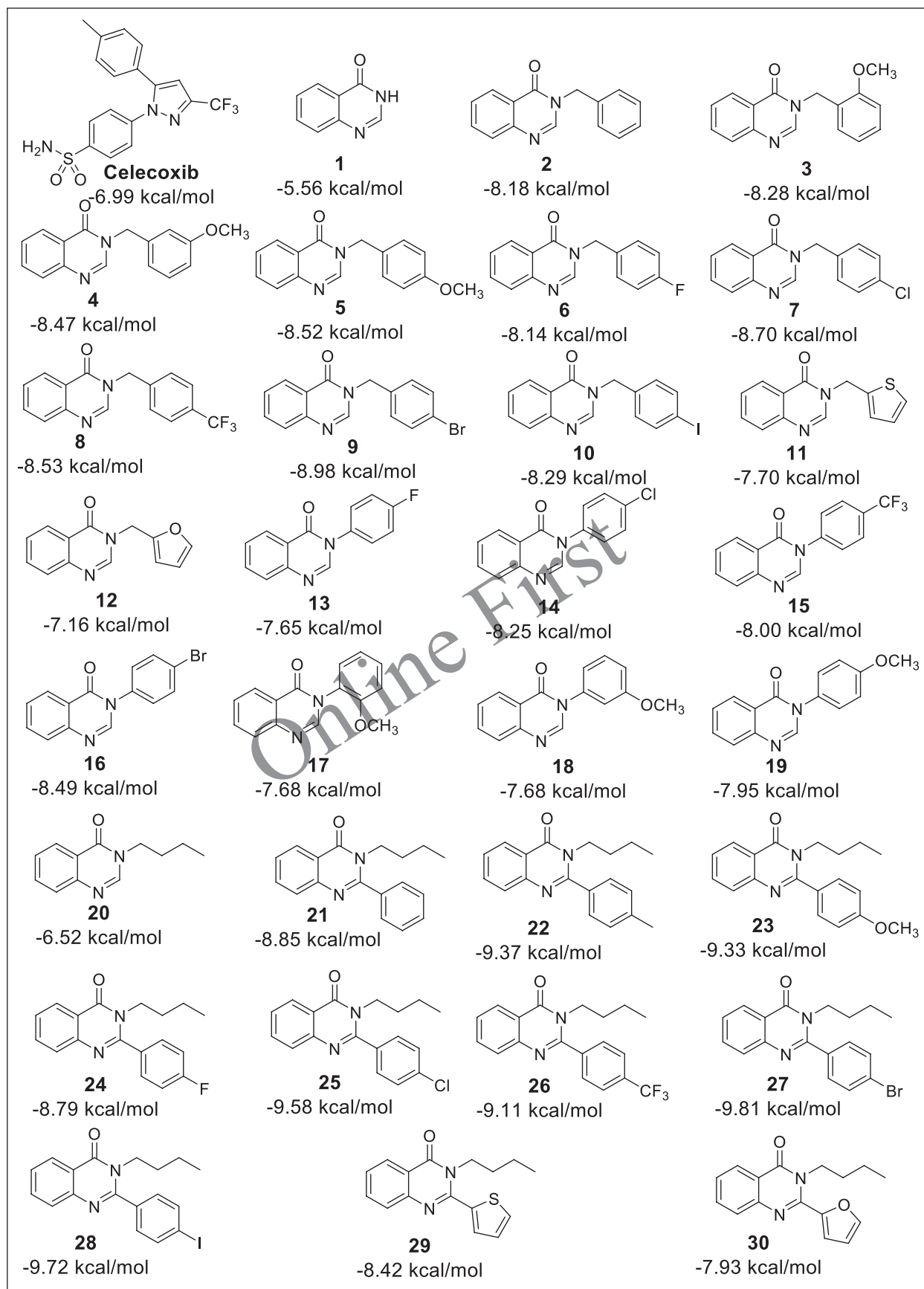
Figure 2. Binding energies for quinazolinone derivatives toward celecoxib in the molecular docking study.
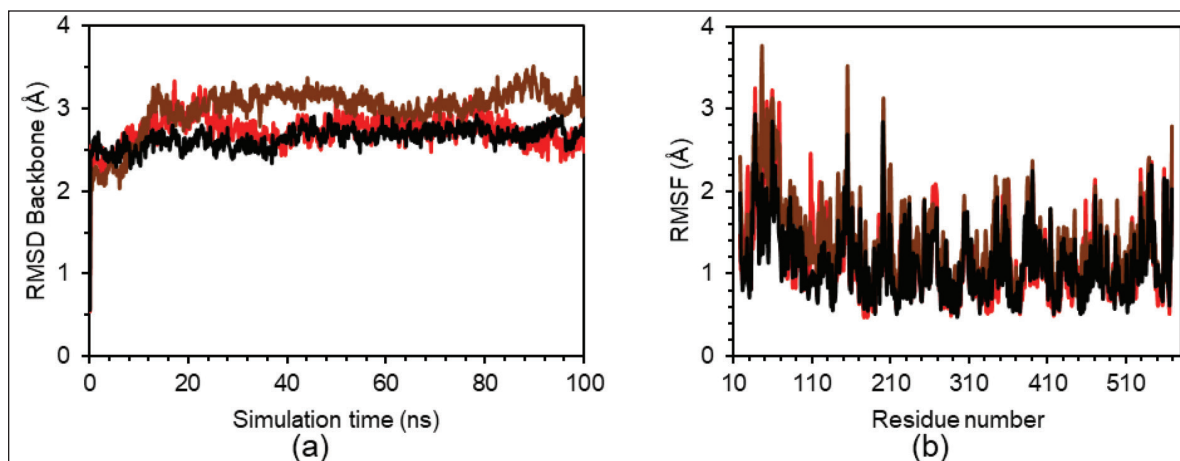
Figure 3. (a) RMSD of the backbone and (b) RMSF during 100 ns simulation for compound **5** (red line), compound **8** (brown line), and celecoxib (black line) against COX-2.

of COX-2 agreed with the Ramachandran data, indicating that each helix, sheet, turn, coil, helix310, and helixPi fraction of COX-2 remained stable during the 100 ns molecular dynamics simulations (Fig. 5).

The RoG value represents the compactness of the enzyme complexed with quinazolinones. Figure 6(a) shows that the RoG values of compound **5**, **8**, and celecoxib were 24.545 ± 0.098, 24.578 ± 0.083, and 24.461 ± 0.069 Å, respectively. These values were not significantly different and remained relatively stable during the molecular dynamics simulations. On the other hand, the SASA value indicates the accessible surface area of the enzyme complex for each ligand. As presented in Figure 6(b), the SASA data for compound **5**, **8**, and celecoxib were 23939 ± 311, 23818 ± 325, and 23089 ± 285 nm². These values align with the RoG value, which was stable during the molecular dynamics simulations.

The chemical interactions of compounds **5** and **8** before and after molecular dynamics simulations are displayed in Figure 7. Initially, compound **5** generated a hydrogen bond with His75 and Arg499 residues, a carbon–hydrogen bond with Phe504 and Val509, a pi-sigma with Ser339, and pi-pi T-shaped interactions with Leu338 and Trp373. After 100 ns of simulation, compound **5** still interacted with His75 through a hydrogen bond. The other interactions, including the carbon–hydrogen bond with Val509 and the pi-sigma interaction with Ser339, also remained. In addition, another hydrogen bond with the Arg106 residue and carbon–hydrogen bonds with Gln178, Leu338, Gly512, and Ser516 residues were formed after 100 ns of simulation. A pi-alkyl interaction with Leu338 and van der Waals interactions with Val335, Tyr341, Phe367, Leu370, Tyr371, Trp373, Ala502, Ile503, Phe504, Met508, and Ala513 residues were also found. These newly formed interactions contributed to a higher binding energy calculated by the MM-PBSA method (Table 2) compared to the molecular docking binding energy (−8.52 kcal/mol).

On the other hand, compound **8** interacted with His75, Ile503, and Phe504 residues through hydrogen bonds in the active site of COX-2. Compound **8** also made interactions with Gln178, Leu338, and Ser339 through halogen (fluorine) bonds,

with Val509 through pi-sigma interaction, with Tyr371 and Trp373 through pi-pi T-shaped interactions, with His75, Val335, Leu338, Ala502, and Val509 through pi-alkyl interactions, and with Tyr341, Phe367, Leu370, Arg499, Met508, Gly512, and Ser516 through van der Waals forces. After molecular dynamics simulations, the hydrogen bonds with His75, Ile503, and Phe504 residues and the pi-sigma interaction with Val509 disappeared, while the halogen (fluorine) bond was found only for the Ala513 residue. In contrast, new carbon–hydrogen interactions with Arg106, pi-pi T-shaped interactions with Phe504 and Met508, pi-alkyl interactions with Arg106, Leu345, and Ala513, and van der Waals interactions with Val102, Leu103, Val335, Ser339, Tyr371, Trp373, and Leu517 were observed for compound **8** in the active site of the COX-2 enzyme. These newly formed interactions contributed to the higher binding energy of compound **8** calculated by the MM-PBSA method (Table 2) compared to the molecular docking binding energy (−8.53 kcal/mol).

Based on the results, compound **5** exhibits significantly better stability and binding efficacy compared to compound **8** (Table 1), as evidenced by post-simulation interactions and energy calculations. While both compounds initially showed strong binding to COX-2, compound **5** retained critical interactions (e.g., hydrogen bonds with His75 and Arg499, carbon–hydrogen bonds with Val509, and pi-sigma interactions with Ser339) after 100 ns of MD simulation. In addition, it formed new stabilizing interactions (hydrogen bond with Arg106, carbon–hydrogen bonds with Gln178/Leu338/Gly512/ Ser516, and pi-alkyl/van der Waals contacts), resulting in a higher MM-PBSA binding energy (−63.25 kcal/mol) compared to its initial docking energy (−8.52 kcal/mol).

In contrast, compound **8** lost key hydrogen bonds with His75, Ile503, and Phe504 during MD simulation, and its halogen bonds with Gln178/Leu338/Ser339, as well as the pi-sigma interaction with Val509, disappeared. Although it formed new interactions (e.g., carbon–hydrogen bonds with Arg106 and pi-alkyl contacts with Leu345/Ala513), these were insufficient to compensate for the loss of critical binding residues. Despite a similar MM-PBSA energy (−62.89 kcal/mol), the instability
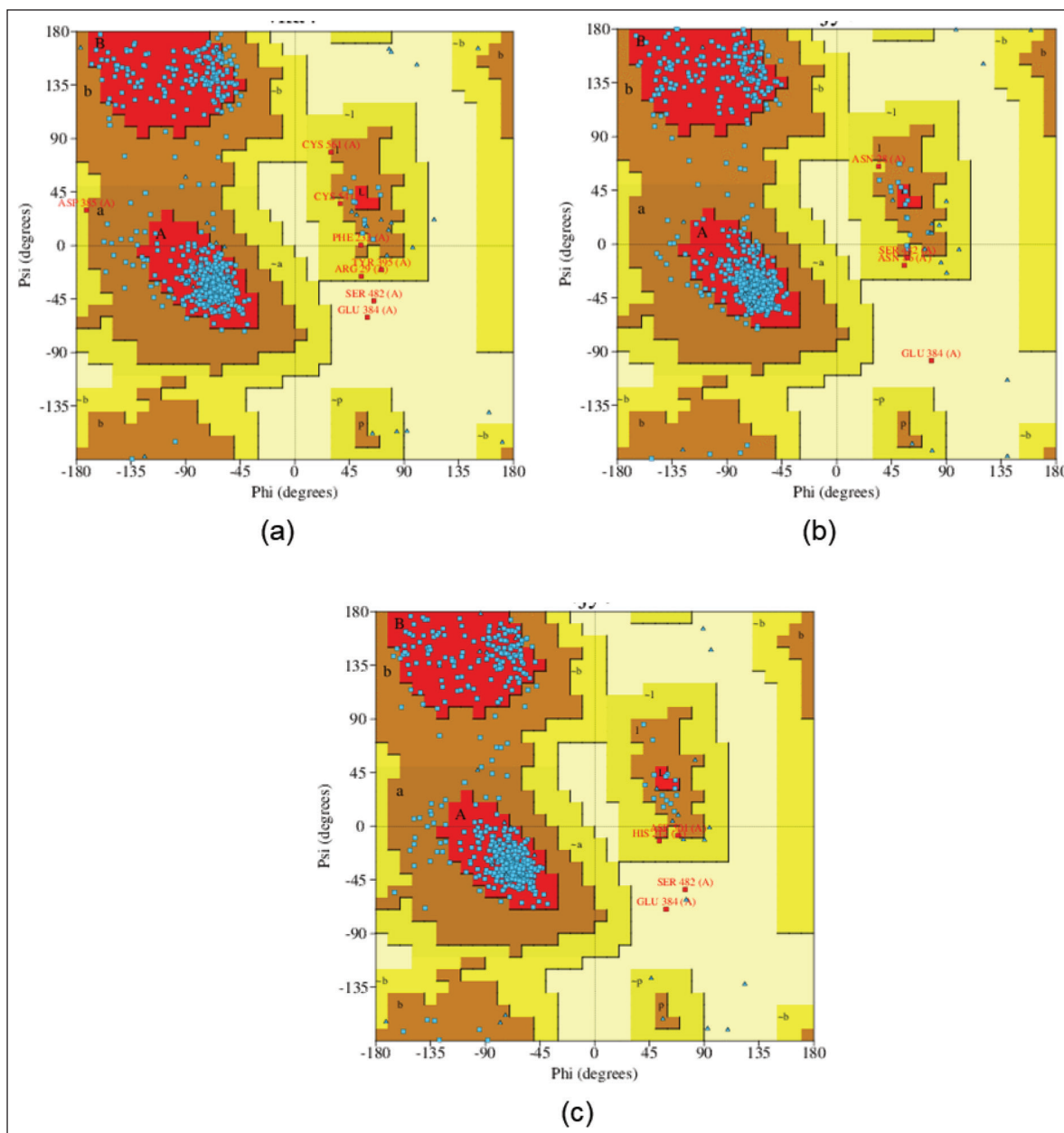
Figure 4. Ramachandran plot for (a) compound **5**, (b) compound **8**, and (c) celecoxib against COX-2.

of compound **8**'s binding pose and its failure to maintain interactions with catalytic residues (e.g., His75) underscore its inferiority to compound **5**.

The retained and newly formed interactions in compound **5** align with the COX-2 active site's pharmacophoric requirements, particularly the conserved His75 and Arg499 residues, which are critical for prostaglandin biosynthesis. This structural consistency, coupled with lower RMSD fluctuations (2.726 ± 0.209 Å *vs.* 2.934 ± 0.346 Å for compound **8**), solidifies compound **5** as a more promising COX-2 inhibitor candidate.

Further ADMET analysis (Table 3) was also performed to evaluate the drug-likeness and pharmacology parameters of quinazolinone derivatives. Neither compound **5** nor compound

8 violates the Lipinski rule as their molecular weight were less than 500 g/mol, their log p values are less than 5, their H-bond donors are fewer than 5, and their H-bond acceptors are less than 10. Furthermore, none of these compounds violate the Egan, Veber, and Ghose rules because their log p values are less than 5.6, topological surface areas are less than 130 Å^2, and rotatable bonds are less than 10. These results indicate the high suitability of quinazolinones from the perspective of drug-likeness parameters. From the absorption parameters, compound **5** demonstrates medium water solubility of −3.647, with the highest %human intestinal absorption (HIA) value of 99.634 and a Caco-2 permeability value of 1.291. Compound **8** also exhibits an acceptable %HIA value of 96.199, with higher Caco-2 permeability than compounds 1 and 5. This indicates that
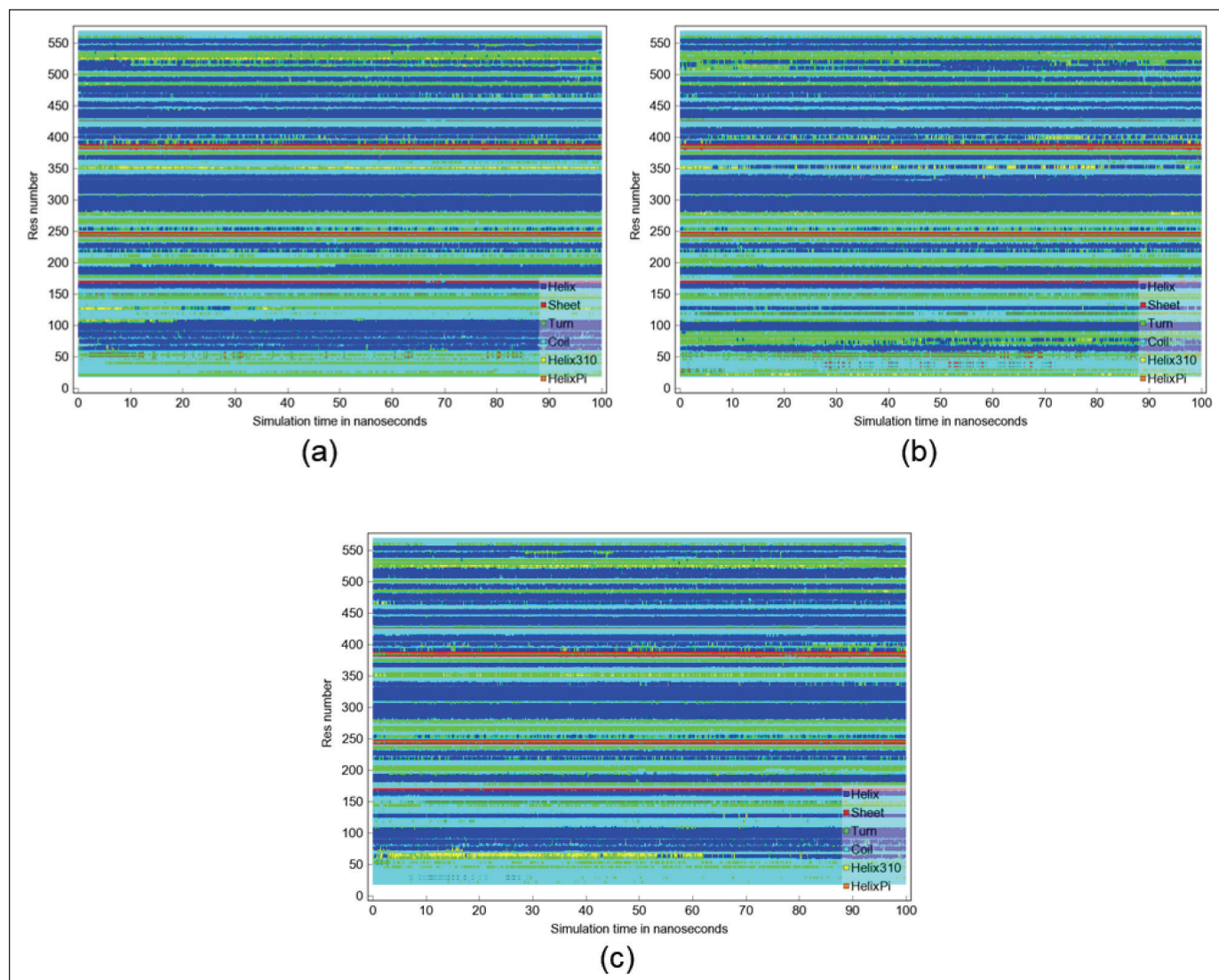
Figure 5. DSSP analysis for (a) compound **5**, (b) compound **8**, and (c) celecoxib against COX-2.

compounds **5** and **8** demonstrate preferable oral absorption with good in vitro drug absorption in the human intestinal mucosa.

The distribution parameters of quinazolinones showed that only compound **8** could cross the blood–brain barrier (BBB) as its log BBB values were higher than 0.3. On the other hand, the presence of methoxy and trifluoromethyl substituents also increased the steady-state volume distribution (VDss) values compared with unmodified and benzylated quinazolinones. The central nervous system (CNS) permeability values of all evaluated quinazolinones were higher than −2, demonstrating that they could penetrate the CNS. From the metabolism point of view, compound **5** was an active inhibitor for two cytochromes, while compound **8** was active for one cytochrome. Unfortunately, the total clearance of compound **8** was the lowest, which was unfavorable. Compound **5** yielded a total clearance value 3.82 times higher than compound **8**. Both compounds **5** and **8** were renal OCT2 substrates; thus, they were predicted to be excreted from the kidneys. Neither of the quinazolinone derivatives generated any cytotoxicity,

mutagenicity, hepatotoxicity, or cardiotoxicity problems. The addition of a benzyl group to quinazolinone demarcated the LD_{50} value from 2.220 to 1.834 mol/kg. However, the presence of methoxy and trifluoromethyl substituents at the para position could recover the LD_{50} from 1.834 to 2.074 and 2.219 mol/kg, respectively. These ADMET data showed that the pharmacokinetic parameters of either compound **5** or compound **8** were sufficient to be tested in experimental works. Importantly, the high clearance rate of compound **5**, combined with the absence of predicted hepatotoxicity, strongly supports its potential as a lead compound for further development.

In this study, not all DFT-B3LYP-6-31G(d,p) methods are suitable for optimizing the proposed structures, especially when functional groups like iodine (I) are present. This can affect the accuracy of structural optimization and the predicted interaction with the COX-2 protein. Based on the analysis of hydrogen bonds, the benzyl-substituted derivatives bearing electron-donating methoxy groups (-OCH$_3$) and electron-withdrawing trifluoromethyl groups (-CF$_3$) exhibited
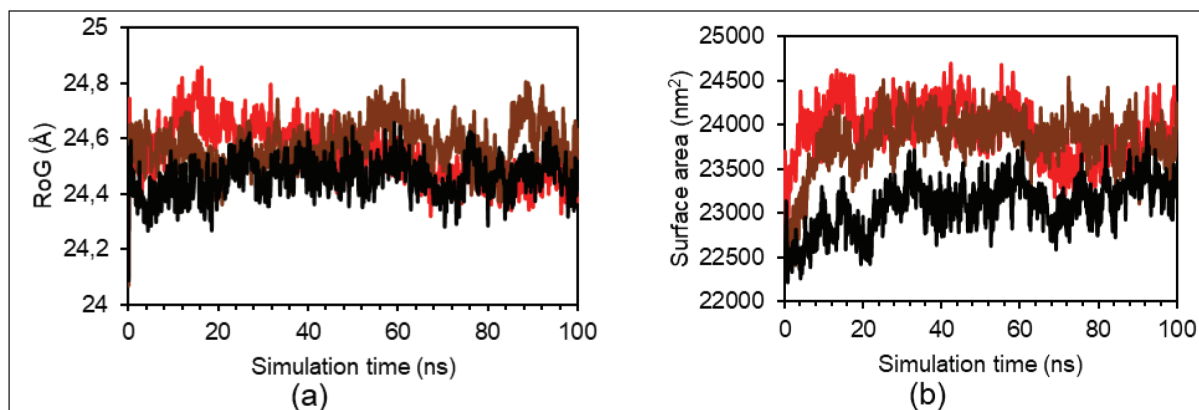
Figure 6. (a) RoG of the backbone and (b) SASA during 100 ns simulation for compound **5** (red line), compound **8** (brown line), and celecoxib (black line) against COX-2.
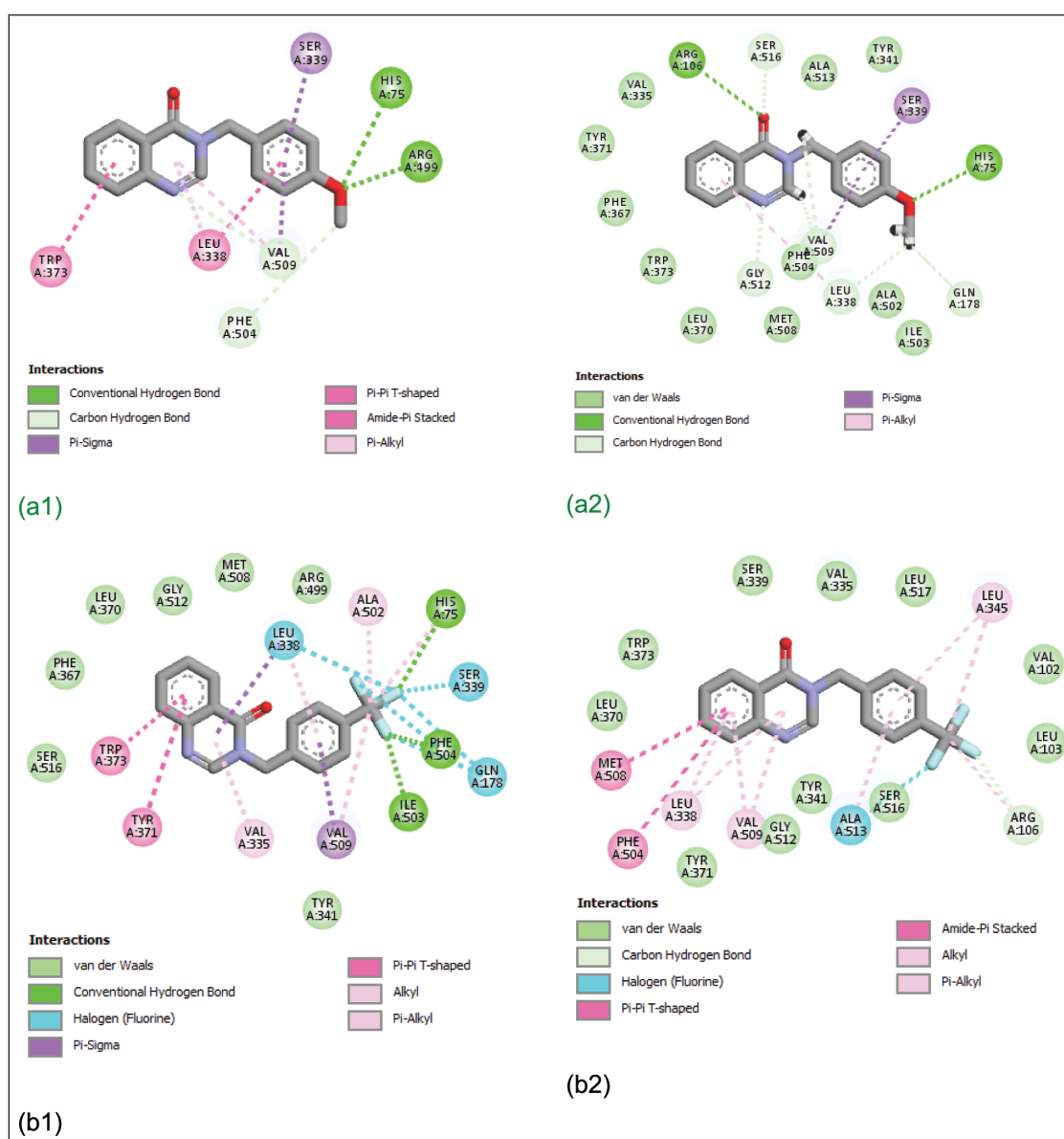

Figure 7. The structures of compound 5 (a1) and compound 8 (b1) before, and compound 5 (a2) and compound 8 (b2) after molecular dynamics simulations within the active site of COX-2.

Table 2. MMPBSA calculation for compound 5, compound 8, and celecoxib after molecular dynamics simulations in the active site of COX-2.

Energy	Energy value (kJ/mol)		
	Compound 5	**Compound 8**	**Celecoxib**
EpotRecept+	−19016.71 ± 1311.25	−17983.07 ± 1426.49	−18981.07 ± 1255.70
EsolvRecept+	−37500.39 ± 1207.36	−38483.43 ± 1379.99	−37175.35 ± 1028.22
EpotLigand+	−139.47 ± 18.62	−60.29 ± 17.17	−228.61 ± 19.35
EsolvLigand−	−52.40 ± 3.76	−53.47 ± 3.48	−175.79 ± 13.13
EpotComplex−	−19366.26 ± 1314.17	−18222.05 ± 1424.12	−19546.64 ± 1266.05
EsolvComplex	−37380.19 ± 1201.48	−38440.53 ± 1383.22	−16160.23 ± 1049.14
Binding energy	37.49 ± 28.02	82.33 ± 33.50	15.18 ± 31.42

Table 3. ADMET results of quinazolinones.

Pharmacokinetic parameter	Compound 5	Compound 8
Drug-likeness		
Molecular weight (g/mol)	266.30	304.27
Log P	2.45	3.46
H-bond donor	0	0
H-bond acceptor	3	5
Topological polar surface area (Å^2)	44.12	34.89
Rotatable bonds	3	3
Absorption		
Water solubility (log mol/l)	−3.647	−4.596
HIA (%)	99.634	96.199
		1.484
Caco-2 permeability (cm/s)	1.291	
Distribution		
log BBB permeability	0.151	0.410
VDss for human	0.068	0.026
CNS permeability	−1.465	−1.328
Metabolism		
CYP2D6 inhibitor	Inactive	Inactive
CYP2E1 inhibitor	Inactive	Inactive
CYP3A4 inhibitor	Active	Inactive
CYP2C9 inhibitor	Active	Inactive
CYP2C19 inhibitor	Inactive	Active
CYP1A2 inhibitor	Inactive	Inactive
Excretion		
Total clearance (log ml/min/kg)	0.630	0.165
Renal OCT2 substrate	Yes	Yes
Toxicity		
Cytotoxicity	Inactive	Inactive
Mutagenicity	Inactive	Inactive
Hepatotoxicity	Inactive	Inactive
Cardiotoxicity	Inactive	Inactive
hERG I inhibitor	No	No

Pharmacokinetic parameter	Compound 5	Compound 8
Drug-likeness		
hERG II inhibitor	No	No
LD$_{50}$ (mol/kg)	2.074	2.219

the strongest and most stable hydrogen bond interactions with key residues in the COX-2 active sites. In contrast, other functional groups such as aryl, heterocyclic, and alkyl substituents showed weaker potential for hydrogen bonding with COX-2, resulting in less effective interactions. These limitations highlight the need for further optimization of computational methods and broader exploration of functional groups to enhance the accuracy and efficacy of molecular designs targeting COX-2 inhibition.

4. CONCLUSION

In this work, quinazolinones were evaluated as COX-2 inhibitors through molecular docking and molecular dynamics simulations. The unsubstituted quinazolinone (compound **1**) yielded a binding energy of −5.56 kcal/mol with a hydrogen bond to the Tyr341 amino acid residue. The addition of the benzyl group on R1 of quinazolinone remarkably increased the binding energy of compound **2** (−8.18 kcal/mol) compared to the unmodified compound (−5.56 kcal/mol). However, compound 2 did not exhibit any hydrogen bonds in the active site of the COX-2 enzyme. The addition of the methoxy and trifluoromethyl groups in compound **2** at the para positions exhibited binding energy of −8.52 and −8.53 kcal/mol. Compound **5** interacted via hydrogen bonds with His75 and Arg499, while compound **8** generated three hydrogen bonds with His75, Ile503, and Phe504. Based on the molecular docking results, compounds **5** and **8** demonstrated the best performance as potential candidates. The molecular dynamics simulation was performed at 310 K for 100 ns. The RMSD, RMSF, RoG, and SASA values of compounds **5** and **8** reached a plateau after 20 ns. Ramachandran analysis showed that more than 80% of the amino acid residues were located in the most favored regions, demonstrating the stability of the COX-2 protein structure as supported by DSSP results.

After 100 ns of simulation, compound **5** still interacted with His75 through hydrogen bonds, while compound **8** lost all of its hydrogen bonds. This finding agreed with the MM-PBSA binding energy, indicating that compound **5** had a stronger interaction than compound **8**. On the other hand, ADMET analysis showed that all quinazolinones did not violate Lipinski, Egan, Veber, and Ghose rules and exhibited good pharmacokinetic properties. Compound **5** showed a higher %HIA value of 99.634 and a total clearance value 3.82 times higher than that of compound **8**.

5. ACKNOWLEDGMENT

6. AUTHORS CONTRIBUTIONS

All authors made substantial contributions to conception and design, acquisition of data, or analysis and interpretation of data; took part in drafting the article or revising it critically for important intellectual content; agreed to submit to the current journal; gave final approval of the version to be published; and agree to be accountable for all aspects of the work. All the authors are eligible to be an author as per the International Committee of Medical Journal Editors (ICMJE) requirements/guidelines.

7. CONFLICTS OF INTEREST

The authors report no financial or any other conflicts of interest in this work.

8. ETHICAL APPROVALS

This study does not involve experiments on animals or human subjects.

9. DATA AVAILABILITY

All data generated and analyzed are included in this research article.

10. PUBLISHER'S NOTE

All claims expressed in this article are solely those of the authors and do not necessarily represent those of the publisher, the editors and the reviewers. This journal remains neutral with regard to jurisdictional claims in published institutional affiliation.

11. USE OF ARTIFICIAL INTELLIGENCE (AI)-ASSISTED TECHNOLOGY

The authors declares that they have not used artificial intelligence (AI)-tools for writing and editing of the manuscript, and no images were manipulated using AI.

REFERENCES

1. Sun X, Liu J, Zhang W, Wang Y, Jiang Y, Wang L, *et al*. Disease burden of biliary tract cancer in 204 countries and territories, 1990– 2021: a comprehensive demographic analysis of the Global Burden of Disease Study 2021. Chin Med J. 2024;137:3117–25. doi: https://doi.org/10.1097/CM9.0000000000003395

2. Cancer n.d. [cited 2025 March 12]. Available from: https://www.who.int/health-topics/cancer#tab=tab_1

3. Ghebremedhin A, Athavale D, Zhang Y, Yao X, Balch C, Song S. Tumor-associated macrophages as major immunosuppressive cells in the tumor microenvironment. Cancers. 2024;16:3410. doi: https://doi.org/10.3390/cancers16193410

4. Bray F, Laversanne M, Sung H, Ferlay J, Siegel RL, Soerjomataram I, *et al*. Global cancer statistics 2022: GLOBOCAN estimates of incidence and mortality worldwide for 36 cancers in 185 countries. CA Cancer J Clin. 2024;74:229–63. doi: https://doi.org/10.3322/caac.21834

5. Rejinthala S, Endoori S, Thumma V, Mondal T. New imidazo[4,5-c]pyridine-piperidine hybrids as potential anti-cancer agents and *in-silico* Studies. Chem Select. 2024;9. doi: https://doi.org/10.1002/slct.202303299

6. Joukhan A, Kononenko V, Bele T, Sollner Dolenc M, Peigneur S, *et al*. Attenuation of nicotine effects on A549 lung cancer cells by synthetic α7 nAChR antagonists APS7-2 and APS8-2. Mar Drugs. 2024;22:147. doi: https://doi.org/10.3390/md22040147

7. Chandraghatgi R, Ji H-F, Rosen GL, Sokhansanj BA. Streamlining computational fragment-based drug discovery through evolutionary optimization informed by ligand-based virtual prescreening. J Chem Inf Model. 2024;64:3826–40. doi: https://doi.org/10.1021/acs.jcim.4c00234

8. Parikh RV, Pandya DV, Salaria P, Amarendar RM, Vyas VK, Bhatt HG, *et al*. Investigation on anti-plasmodial agents against wild-type *Pf* DHFR through *in silico* computational tools. Chem Select. 2024;9. doi: https://doi.org/10.1002/slct.202304151

9. Aswathy M, Parama D, Hegde M, Sherin DR, Lankalapalli RS, Radhakrishnan KV, *et al*. Natural prenylflavones from the stem bark of *Artocarpus altilis*: promising anticancer agents for oral squamous cell carcinoma targeting the Akt/mTOR/STAT-3 signaling pathway. ACS Omega. 2024;9:24252–67. doi: https://doi.org/10.1021/acsomega.3c08376

10. Astaneh ME, Fereydouni N. Silver nanoparticles in 3D printing: a new frontier in wound healing. ACS Omega. 2024;9:41107–29. doi: https://doi.org/10.1021/acsomega.4c04961

11. Sestito S, Ibba R, Riu F, Carpi S, Carta A, Manera C, *et al*. Anticancer potential of decursin, decursinol angelate, and decursinol from *Angelica gigas* nakai: a comprehensive review and future therapeutic prospects. Food Sci Nutr. 2024;12:6970–89. doi: https://doi.org/10.1002/fsn3.4376

12. Zhang G, Xu Y, Zhou A, Yu Y, Ning X, Bao H. Bioengineered nano aid synergistically targets inflammatory pro-tumor processes to advance glioblastoma chemotherapy. Nanoscale. 2025;17:2753–68. doi: https://doi.org/10.1039/D4NR04557B

13. Hussain S, Iqbal A, Hamid S, Putra PP, Ashraf M. Identifying alkaline phosphatase inhibitory potential of cyclooxygenase-2 inhibitors: Insights from molecular docking, MD simulations, molecular expression analysis in MCF-7 breast cancer cell line and *in vitro* investigations. Int J Biol Macromol. 2024;277:132721. doi: https://doi.org/10.1016/j.ijbiomac.2024.132721

14. Neha K, Singh G, Singh M, Asthana S, Wakode S. *In silico* strategies to recognize pharmacological constraints contrary to COX-2 and 5-LOX. J Biomol Struct Dyn. 2024;2024:1–18. doi: https://doi.org/10.1080/07391102.2024.2425404

15. Ishaniya W, Sugantharam K, Subramani M, Kumar AM, Gopinath P, Rajendran S, *et al*. Lipid-coated mesoporous silica nanoparticles for pH-responsive release and enhanced anti-proliferative activity of piperlongumine natural product. Chem Select. 2024;9. doi: https://doi.org/10.1002/slct.202402022

16. Abd El-Karim SS, Syam YM, El Kerdawy AM, Abdel-Mohsen HT. Rational design and synthesis of novel quinazolinone N-acetohydrazides as type II multi-kinase inhibitors and potential

anticancer agents. Bioorg Chem. 2024;142:106920. doi: https://doi.org/10.1016/j.bioorg.2023.106920

17. Mhetre UV, Haval NB, Bondle GM, Rathod SS, Choudhari PB, Kumari J, *et al*. Design, synthesis and molecular docking study of novel triazole–quinazolinone hybrids as antimalarial and antitubercular agents. Bioorg Med Chem Lett. 2024;108:129800. doi: https://doi.org/10.1016/j.bmcl.2024.129800

18. Mohammadi M, Dilmaghani KA, Sarveahrabi Y. Synthesis, antibacterial, and antifungal evaluation of some new quinazolinone-azole hybrids. Polycycl Aromat Compd. 2024;44:1805–15. doi: https://doi.org/10.1080/10406638.2023.2208706

19. Moftah HK, Mousa MHA, Elrazaz EZ, Kamel AS, Lasheen DS, Georgey HH. Novel quinazolinone derivatives: design, synthesis and *in vivo* evaluation as potential agents targeting Alzheimer disease. Bioorg Chem. 2024;143:107065. doi: https://doi.org/10.1016/j.bioorg.2023.107065

20. Wahan SK, Sharma B, Chawla PA. Medicinal perspective of quinazolinone derivatives: recent developments and structure–activity relationship studies. J Heterocycl Chem. 2022;59:239–57. doi: https://doi.org/10.1002/jhet.4382

21. Verma P, Xiang LZ, Chaube U, Natesan G. Synthesis, antimicrobial evaluation, molecular docking and dynamics simulations of novel 2,3-disubstituted quinazolin-4(3H)-one derivatives. Chem Select. 2024;9. doi: https://doi.org/10.1002/slct.202403009

22. Parmar D, Tripathi RKP, Panchal R, Nagani A, Kabra UD. New quinazolinone-thiouracil derivatives: design, synthesis, anticancer evaluation, and *in silico* analysis. Chem Select. 2024;9. doi: https://doi.org/10.1002/slct.202403717

23. Alkaoud AM, Alakhras AI, Ibrahim MA, Alghamdi SK, Hussein RK. *In silico* evaluation of a new compound incorporating 4(3H)-quinazolinone and sulfonamide as a potential inhibitor of a human carbonic anhydrase. BMC Chem. 2024;18:45. doi: https://doi.org/10.1186/s13065-024-01150-1

24. Chen K, Wang S, Fu S, Kim J, Park P, Liu R, *et al*. 4(3H)-quinazolinone: a natural scaffold for drug and agrochemical discovery. Int J Mol Sci. 2025;26:2473. doi: https://doi.org/10.3390/ijms26062473

25. Abdel-Mohsen HT, Anwar MM, Ahmed NS, Abd El-Karim SS, Abdelwahed SH. Recent advances in structural optimization of quinazoline-based protein kinase inhibitors for cancer therapy (2021–Present). Molecules. 2024;29:875. doi: https://doi.org/10.3390/molecules29040875

26. Pedrood K, Sherafati M, Mohammadi-Khanaposhtani M, Asgari MS, Hosseini S, Rastegar H, *et al*. Design, synthesis, characterization, enzymatic inhibition evaluations, and docking study of novel quinazolinone derivatives. Int J Biol Macromol. 2021;170:1–12. doi: https://doi.org/10.1016/j.ijbiomac.2020.12.121

27. El-Menshawe SF, Sayed OM, Abou Taleb HA, Saweris MA, Zaher DM, Omar HA. The use of new quinazolinone derivative and doxorubicin loaded solid lipid nanoparticles in reversing drug resistance in experimental cancer cell lines: a systematic study. J Drug Deliv Sci Technol. 2020;56:101569. doi: https://doi.org/10.1016/j.jddst.2020.101569

28. Kerdphon S, Khamto N, Buddhachat K, Ngoenkam J, Paensuwan P, Pongcharoen S, *et al*. Structure–activity relationship and molecular docking of quinazolinones inhibiting expression of COX-2, IL-1β, iNOS, and TNF-α through NF-κB pathways. ACS Med Chem Lett. 2023;14:1167–73. doi: https://doi.org/10.1021/acsmedchemlett.3c00098

29. Sakr A, Rezq S, Ibrahim SM, Soliman E, Baraka MM, Romero DG, *et al*. Design and synthesis of novel quinazolinones conjugated ibuprofen, indole acetamide, or thioacetohydrazide as selective COX-2 inhibitors: anti-inflammatory, analgesic and anticancer activities. J Enzyme Inhib Med Chem. 2021;36:1810–28. doi: https://doi.org/10.1080/14756366.2021.1956912

30. Yuli Astuti PD, Fadilah F, Promsai S, Bahtiar A. Integrating molecular docking and molecular dynamics simulations to evaluate active

31. compounds of *Hibiscus schizopetalus* for obesity. J Appl Pharm Sci. 2024;2024. doi: https://doi.org/10.7324/JAPS.2024.158550

31. Situmeang B, Swasono RT, Raharjo TJ. Evaluation of phytochemical composition, antioxidant, cytotoxic and *in silico* studies of ethyl acetate fractions of *Tristaniopsis merguensis* leaves. Toxicol Rep. 2025;14:101911. doi: https://doi.org/10.1016/j.toxrep.2025.101911

32. Ananto AD, Pranowo HD, Haryadi W, Prasetyo N. Flavonoid compound of red fruit papua and its derivatives against SARS-CoV-2 mpro: an *in silico* approach. J Appl Pharm Sci. 2024;2024. doi: https://doi.org/10.7324/JAPS.2024.177392

33. Kurniawan YS, Yudha E, Nugraha G, Fatmasari N, Pranowo HD, Jumina J, *et al*. Molecular docking and molecular dynamic investigations of xanthone-chalcone derivatives against epidermal growth factor receptor for preliminary discovery of novel anticancer agent. Indonesian J Chem. 2024;24:250. doi: https://doi.org/10.22146/ijc.88449

34. Gomaa M, Gad W, Hussein D, Pottoo FH, Tawfeeq N, Alturki M, *et al*. Sulfadiazine exerts potential anticancer effect in HepG2 and MCF7 cells by inhibiting TNFα, IL1b, COX-1, COX-2, 5-LOX gene expression: evidence from *in vitro* and computational studies. Pharmaceuticals. 2024;17:189. doi: https://doi.org/10.3390/ph17020189

35. Fitria A, Kurniawan YS, Ananto AD, Jumina J, Sholikhah EN, Pranowo HD. Allyl-modified of calix[4]resorcinarene derivatives for HER2 inhibition agents: an *in silico* study. J Multidiscipl Appl Nat Sci. 2025;2025. doi: https://doi.org/10.47352/jmans.2774-3047.250

36. Nezhad NG, Borzehandani MY, Eskandari A, Rahman RNZRA, Yahaya NM, Oslan SN, *et al*. A comparative investigation of predicted protein structures of A histidine acid phosphatase from *Saccharomyces cerevisiae* through molecular docking and MD simulations. J Proteins Proteom. 2025;16:35–47. doi: https://doi.org/10.1007/s42485-025-00174-y

37. Nandhini M, Pitchumani Violet Mary C, Gopinath S, Vijayakumar S. Structure-based interaction and molecular dynamics studies of cysteine protease cathepsin B against curcumin and resveratrol. J Biomol Struct Dyn. 2024;2024:1–11. doi: https://doi.org/10.1080/07391102.2024.2431658

38. Chan L-C, Mat Yassim AS, Ahmad Fuaad AAH, Leow TC, Sabri S, Radin Yahaya RS, *et al*. Inhibition of SARS-CoV-2 3CL protease by the anti-viral chimeric protein RetroMAD1. Sci Rep. 2023;13:20178. doi: https://doi.org/10.1038/s41598-023-47511-z

39. Pappalardo M, Sipala FM, Nicolosi MC, Guccione S, Ronsisvalle S. Recent applications of *in silico* approaches for studying receptor mutations associated with human pathologies. Molecules. 2024;29:5349. doi: https://doi.org/10.3390/molecules29225349

40. Zohora FT, Azam ATMZ, Ahmed S, Rahman KM, Halim MA, Anwar MdR, *et al*. Isolation and *in silico* prediction of potential drug-like compounds with a new dimeric prenylated quinolone alkaloid from *Zanthoxylum rhetsa* (Roxb.) root extracts targeted against SARS-CoV-2 (Mpro). Molecules. 2022;27:8191. doi: https://doi.org/10.3390/molecules27238191

41. Laskowski RA, Jabłońska J, Pravda L, Vařeková RS, Thornton JM. PDBsum: structural summaries of PDB entries. Protein Sci. 2018;27:129–34. doi: https://doi.org/10.1002/pro.3289

42. Ezugwu JA, Okoro UC, Ezeokonkwo Mercy A, Hariprasad KS, Rudrapal M, Gogoi N, *et al*. Design, synthesis, molecular docking, drug-likeness/ADMET and molecular dynamics studies of thiazolyl benzenesulfonamide carboxylates as antimalarial agents. Chem Africa. 2024;7:2353–68. doi: https://doi.org/10.1007/s42250-024-00904-7

43. Bendjabeur S, Hazzit M. Antioxidant and anticholinesterase activities, molecular docking, ADMET and drug-likeness studies of essential oil and ethanolic extract from *Ammodaucus leucotrichus* Coss. and Dur. Fruits. J Essent Oil Bear Plants. 2024;27:1492–503. doi: https://doi.org/10.1080/0972060X.2024.2423774

44. Gheidari D, Mehrdad M, Bayat M. Synthesis, docking, MD simulation, ADMET, drug likeness, and DFT studies of novel furo[2,3-b]indol-3a-ol as promising cyclin-dependent kinase 2 inhibitors. Sci Rep. 2024;14:3084. doi: https://doi.org/10.1038/s41598-024-53514-1

45. Pandey SK, Yadava U, Sharma ML, Upadhyay A, Gupt MP, Dwivedi AR, *et al*. Synthesis, molecular structure investigation, biological evaluation and docking studies of novel spirothiazolidinones. Results Chem. 2023;5:100726. doi: https://doi.org/10.1016/j.rechem.2022.100726

46. Kassem AF, Ragab SS, Omar MA, Altwaijry NA, Abdelraof M, Temirak A, *et al*. New quinazolone–sulfonate conjugates with an acetohydrazide linker as potential antimicrobial agents: design, synthesis and molecular docking simulations. RSC Adv. 2025;15:1033–48. doi: https://doi.org/10.1039/D4RA07563C

47. Liu X, Zhang J, Sun W, Cao J, Ma Z. COX-2 in lung cancer: mechanisms, development, and targeted therapies. Chronic Dis Transl Med. 2024;10:281–92. doi: https://doi.org/10.1002/cdt3.120

48. Abdel-Aziz AA-M, El-Azab AS, Brogi S, Ayyad RR, Al-Suwaidan IA, Hefnawy M. Antitumor activity and multi-target mechanism of phenolic schiff bases bearing methanesulfonamide fragments: cell cycle analysis and a molecular modeling study. Int J Mol Sci. 2024;25:13621. doi: https://doi.org/10.3390/ijms252413621

49. El-Sayed NNE, Al-Otaibi TM, Barakat A, Almarhoon ZM, Hassan MohdZ, Al-Zaben MI, *et al*. Synthesis and biological evaluation of some new 3-Aryl-2-thioxo-2,3-dihydroquinazolin-4(1H)-ones and 3-Aryl-2-(benzylthio)quinazolin-4(3H)-ones as antioxidants; COX-2, LDHA, α-glucosidase and α-amylase inhibitors; and anti-colon carcinoma and apoptosis-inducing agents. Pharmaceuticals. 2023;16:1392. doi: https://doi.org/10.3390/ph16101392

50. Liu X, Zhang J, Sun W, Cao J, Ma Z. COX-2 in lung cancer: mechanisms, development, and targeted therapies. Chronic Dis Transl Med 2024;10:281–92. doi: https://doi.org/10.1002/cdt3.120

51. Abdel-Aziz AA-M, El-Azab AS, Brogi S, Ayyad RR, Al-Suwaidan IA, Hefnawy M. Antitumor activity and multi-target mechanism of phenolic schiff bases bearing methanesulfonamide fragments: cell cycle analysis and a molecular modeling study. Int J Mol Sci 2024;25:13621. doi: https://doi.org/10.3390/ijms252413621

52. El-Sayed NNE, Al-Otaibi TM, Barakat A, Almarhoon ZM, Hassan MohdZ, Al-Zaben MI, *et al*. Synthesis and biological evaluation of some new 3-Aryl-2-thioxo-2,3-dihydroquinazolin-4(1H)-ones and 3-Aryl-2-(benzylthio)quinazolin-4(3H)-ones as antioxidants; COX-2, LDHA, α-Glucosidase and α-Amylase inhibitors; and anti-colon carcinoma and apoptosis-inducing agents. Pharmaceuticals 2023;16:1392. doi: https://doi.org/10.3390/ph16101392